N-tert-butoxycarbonyl (BOC) protected [V$_6$O$_{13}${(OCH$_2$)$_3$CNH$_2$}$_2$]$^{2-}$: synthesis, structural characterization, and solution behavior

Ibrahima Fa Bamba , Clément Falaise , Gildas K. Gbassi , Patrick Atheba , Mohamed Haouas & Emmanuel Cadot

View supplementary material ☐

Published online: 12 Oct 2020.

Submit your article to this journal ☐

View related articles ☐

View Crossmark data ☐

Check for updates

N-tert-butoxycarbonyl (BOC) protected [V$_6$O$_{13}${(OCH$_2$)$_3$CNH$_2$}$_2$]$^{2-}$: synthesis, structural characterization, and solution behavior

Ibrahima Fa Bamba[a], Clément Falaise[a], Gildas K. Gbassi[b], Patrick Atheba[b], Mohamed Haouas[a] and Emmanuel Cadot[a]

[a]Institut Lavoisier de Versailles, CNRS, UVSQ, Université Paris-Saclay, Versailles, France; [b]UFR Sciences Pharmaceutiques et Biologiques (UFR SPB), Université Félix Houphouet Boigny (UFHB), Abidjan, Côte d'Ivoire

ABSTRACT

Herein, we report the synthesis of N-tert-butoxycarbonyl (BOC) protected [V$_6$O$_{13}${(OCH$_2$)$_3$C–NH$_2$}$_2$]$^{2-}$ built from the Lindqvist-type hexavanadate. The reaction of di-tert-butyl dicarbonate (BOC$_2$O) with tris(hydroxymethyl)aminomethane (Tris) led to the organic derivative [(OCH$_2$)$_3$C–NH(BOC)] that reacts with the decavanadate in dimethylacetamide (DMA) to form the [V$_6$O$_{13}${(OCH$_2$)$_3$C–NH(BOC)}$_2$]$^{2-}$ anion. The tetrabutylammonium (TBA$^+$) salt of this hybrid polyoxovanadate, TBA$_2$[V$_6$O$_{13}${(OCH$_2$)$_3$C–NH(BOC)}$_2$]· 2DMA, has been characterized in the solid-state by single-crystal X-ray diffraction and infrared spectroscopy, and in solution by multinuclear (^{1}H, ^{13}C, ^{15}N and ^{51}V) and DOSY NMR, and UV–visible spectroscopy.
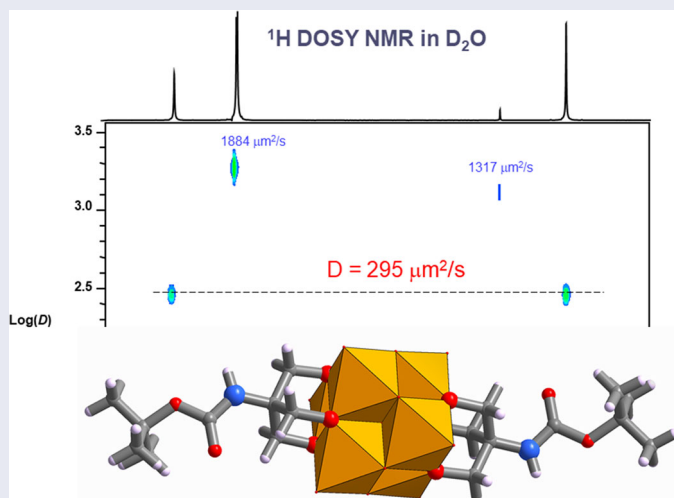
1. Introduction

The need of redox-active molecular components to develop functional systems relevant in the field of energy has led to a renewal of interest for the chemistry of the polyoxovanadates (POVs). POVs, that represent a sub-class of the polyoxometalates (POMs), are anionic molecular oxides exhibiting a rich structural chemistry due to the ability of the vanadium to adopt different oxidation states (V^{IV} and V^{V}) and coordination geometries such as $[VO_4]$, $[VO_5]$, or $[VO_6]$ [1, 2]. The growing interest for POVs is mainly due to their striking redox and catalytic properties making POVs particularly appealing for both fundamental and applied studies related to redox-flow batteries [3–6], lithium or sodium-ion batteries [7–10], water oxidation catalysis [11, 12], or photocatalysis [13]. Recently, it was also demonstrated that POVs constitute excellent models to study the intriguing properties of vanadium solid-state oxides [14–16].

Another attractive feature of POVs is their propensity to form a wide variety of covalent organic-inorganic hybrids, offering a way to i) tune the POV properties and ii) integrate POVs into functional systems or materials [17, 18]. The most studied hybrid POVs are the bis(triol-ligands)-substituted Lindqvist-type hexavanadates, *trans*-$[V_6O_{13}\{(OCH_2)_3CR\}_2]^{2-}$, that exhibit fascinating redox [19, 20], supramolecular [21–24], and photochemical [25] properties. In the early 1990s, the pioneering work of Zubieta demonstrated that reaction of various triol-ligands with decavanadate anion $[V_{10}O_{28}]^{6-}$ in acetonitrile led to the formation of $[V_6O_{13}\{(OCH_2)_3C–R\}_2]^{2-}$ with various functional groups $R = NO_2$, CH_2OH, CH_3 [19, 26, 27]. Later, Müller reported the pentaerythritol derivative ($R = CH_2OH$) can be also prepared in high yield from aqueous mixtures [28]. The $[V_6O_{13}\{(OCH_2)_3C–CH_2OH\}_2]^{2-}$ anion has been used as a platform for various post-functionalizations [29, 30]. The use of $–NH_2$ as functional group is also convenient for post-functionalization of POMs [17, 21, 22, 31, 32], however, it is difficult to obtain $[V_6O_{13}\{(OCH_2)_3C–NH_2\}_2]^{2-}$ by reacting tris(hydroxymethyl)aminomethane (Tris) with vanadate precursors. Indeed the direct reaction of Tris with decavanadate in dry dimethylacetamide (90 °C overnight) led to the desired compound with a very low yield (<6%) [21]. To tackle this issue, the group of Wei successfully isolated the $[V_6O_{13}\{(OCH_2)_3C–NH_2\}_2]^{2-}$ anion in good yield (53%) employing a two-step process strategy. First, the amino group is protected with 4-anisaldehyde prior to grafting reaction and then hydrolysis of formed imine is achieved to recover the amine function [33].

Alternatively, N-tert-butoxycarbonyl group (BOC) is now ranked as "one of the most commonly used protective groups for amines" [34]. Such BOC-based methodology derives from that reported by Wei *et al*. but in this case, the organic precursor corresponding to the BOC-protected Tris compound is synthesized straightforwardly in methanol through a one-pot procedure leading to a 100% yield while the oxazolidine derivatives were obtained from toluene with a lower yield (about 60%) after purification [35]. Then, we show that synthesis methodology based on BOC protecting group corresponds to an efficient and straightforward route to get the Tris-substituted Lindqvist POV $[V_6O_{13}\{(OCH_2)_3C–NH_2\}_2]^{2-}$ in good yield (50%). The novel hybrid anion, $[V_6O_{13}\{(OCH_2)_3C–NH(BOC)\}_2]^{2-}$, isolated as tetra-n-butylammonium (TBA$^+$) salt has been characterized by single-crystal X-ray diffraction, infrared, UV–vis and multinuclear NMR (^{1}H, ^{13}C, and ^{51}V) spectroscopy.

2. Experimental

2.1. Materials

All chemicals were used as received without any further treatment. The precursors $(TBA)_3[H_3V_{10}O_{28}]$ and tert-butyl N-[1,3-dihydroxy-2-(hydroxymethyl)propan-2-yl]carbamate were synthesized and characterized following published procedures [36, 37].

2.2. Preparation of $TBA_2[V_6O_{13}\{(OCH_2)_3C–NH(BOC)\}_2]\cdot2DMA$

$TBA_3[H_3V_{10}O_{28}]$ (6.24 g, 3.7 mmol) and tert-butyl N-[1,3-dihydroxy-2-(hydroxymethyl)-propan-2-yl]carbamate (2.49 g, 11.2 mmol) were dissolved in 75 ml of N,N-dimethylacetamide (DMA). The resulting orange solution was heated at 80 °C for 48 h. After cooling to room temperature, slow diffusion of the solution (red-orange) in ether led to the formation of 5 g of red needles of $TBA_2[V_6O_{13}\{(OCH_2)_3C–NH(BOC)\}_2]\cdot2DMA$ (notated **V_6-Tris-BOC**) which are then isolated by filtration and dried in air. Yield: 50% based on vanadium. Anal. Calcd. (found) for $C_{56}H_{122}N_6O_{25}V_6$: C, 42.4(42.3); H, 7.7(7.4); N, 5.3(5.1); V, 19.3(18.9).

2.3. Preparation of $Na_2[V_6O_{13}\{(OCH_2)_3C–NH(BOC)\}_2]\cdot6H_2O$

Five hundred milligrams of $TBA_2[V_6O_{13}\{(OCH_2)_3C–NH(BOC)\}_2]\cdot2DMA$ (0.31 mmol) were dissolved in 10 ml of acetonitrile. Then this reddish solution was dropped into 5 mL of acetonitrile containing 2 g of sodium perchlorate hydrate (16 mmol) under stirring. Immediately after the addition of the first drops, a dark orange precipitate formed. The resulting mixture is stirred for 2 h. 350 mg of $Na_2[V_6O_{13}\{(OCH_2)_3C–NH(BOC)\}_2]\cdot6H_2O$ (0.27 mmol) is recovered by centrifugation (5000 rpm) and washed with acetonitrile and diethyl ether. Yield: 87% based on vanadium. Anal. Calcd. (found) for $C_{18}H_{44}N_2Na_2O_{29}V_6$: C, 19.7(18.6); H, 4.0(4.25); N, 2.5(2.6); Na, 4.16(3.97); V, 27.7(25.7).

2.4. Preparation of $[V_6O_{13}\{(OCH_2)_3C–NH_3\}_2]\cdot2H_2O$

Three hundred and fifty milligrams of $Na_2[V_6O_{13}\{(OCH_2)_3C–NH(BOC)\}_2]\cdot6H_2O$ was dissolved in 15 mL of water, then 5.5 mL of concentrated HCl (37%) were slowly added, provoking formation of a reddish precipitate. After one day of stirring, the resulting solid is recovered by centrifugation and washed twice with acetonitrile. The dried solids were added to about 10 mL of DI water and ammonia aqueous solution (25%) was added to obtain a clear solution (pH $\sim$ 9). The evaporation of this solution led to the crystallization of $[V_6O_{13}\{(OCH_2)_3C–NH_3\}_2]\cdot2H_2O$. Single-crystal X-ray diffraction reveals that the crystal exhibits the same unit cell as the compound reported previously by Wei and co-workers [33].

2.5. Single-crystal X-ray diffraction

A crystal of **V_6-Tris-BOC** was selected under polarizing optical microscope and glued in paratone oil. X-ray intensity data were collected at low temperature ($T = 220(2)$ K)

Table 1. Crystal data and structure refinement for V_6-Tris-BOC.

Empirical formula	$C_{58}H_{122}N_6O_{25}V_6$
Formula weight	1607.23
Temperature/K	220
Crystal system	Monoclinic
Space group	$P2_1/c$
a/Å	14.8061(3)
b/Å	10.8895(3)
c/Å	24.3085(6)
α/°	90
β/°	101.0590(10)
γ/°	90
Volume/Å^3	3846.50(16)
Z	2
ρ_{calc}g/cm^3	1.388
F(000)	1696
Crystal size/mm^3	$0.16 \times 0.14 \times 0.12$
Radiation	MoKα ($\lambda = 0.71073$)
2Θ range for data collection/°	4.674 to 55.77
Index ranges	$-19 \leq h \leq 19$
	$-14 \leq k \leq 14$
	$-31 \leq l \leq 31$
Reflections collected	81909
Independent reflections	9131
	$R_{int} = 0.0399$
	$R_{sigma} = 0.0192$
Data/restraints/parameters	9131/0/440
Goodness-of-fit on F^2	1.083
Final R indexes [I $\geq 2\sigma$ (I)]	$R_1 = 0.0501$
	$wR_2 = 0.1364$
Final R indexes [all data]	$R_1 = 0.0653$
	$wR_2 = 0.1541$
Largest diff. peak/hole /e Å^{-3}	0.69/−0.45

on a Bruker D8 VENTURE diffractometer equipped with a PHOTON III C14 using a high brilliance IμS microfocus X-ray Mo Kα monochromated radiation ($\lambda = 0.71073$ Å). Data reduction was accomplished using SAINT V7.53a. The substantial redundancy in data allowed a semi-empirical absorption correction (SADABS V2.10) to be applied, on the basis of multiple measurements of equivalent reflections. Using Olex2 [38], the structure was solved with the ShelXT [39] structure solution program using Intrinsic Phasing and refined with the ShelXL [40] refinement package using least squares minimization. The remaining non-hydrogen atoms were located from Fourier differences and were refined with anisotropic thermal parameters. Positions of the hydrogens belonging to $[V_6O_{13}\{(OCH_2)_3C–NH(BOC)\}_2]^{2-}$, TBA$^+$ or DMA were calculated and refined isotropically using the gliding mode. Crystallographic data for single-crystal X-ray diffraction studies are summarized in Table 1. These data can be obtained free of charge from the Cambridge Crystallographic Data Centre via https://www.ccdc.cam.ac. uk/structures-beta/. Deposit number: 2006943.

2.6. NMR studies

The ^1H, $^{13}C\{^1H\}$, $^{15}N\{^1H\}$, and ^{51}V NMR solution spectra were recorded in 5 mm o.d. tubes with a Bruker Avance 400 spectrometer equipped with a BBI probehead. Chemical shifts are referenced to external 1% Me$_4$Si in CDCl$_3$ (^1H and ^{13}C), MeNO$_2$ (^{15}N) and 90% VOCl$_3$ in C$_6$D$_6$ (^{51}V). Translational diffusion measurements were
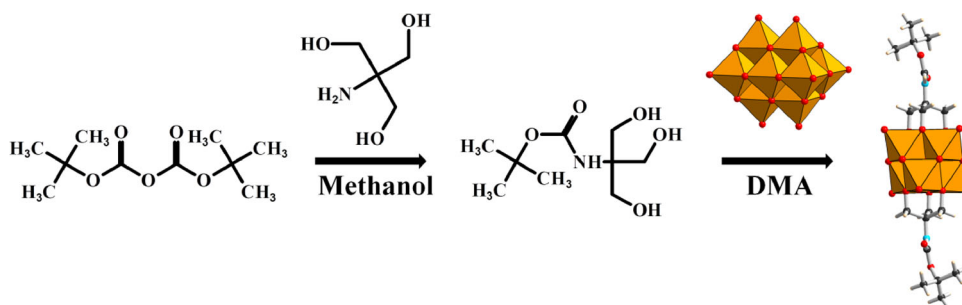
Figure 1. Synthetic pathway leading to $[V_6O_{13}\{(OCH_2)_3C–NH(BOC)\}_2]^{2-}$.

performed using Bruker's "ledbpgs2s" stimulated echo DOSY pulse sequence including bipolar and spoil gradients. Apparent diffusion coefficients were obtained using an adapted algorithm based on the inverse Laplace transform stabilized by maximum entropy [41].

2.7. Fourier transform infrared

Fourier transform infrared (FT-IR) spectra were recorded on a 6700 FT-IR Nicolet spectrophotometer using diamond ATR technique. The spectra were recorded on non-diluted compounds from 400 to 4000 cm^{-1}. ATR correction was applied.

2.8. UV–vis spectra

 The UV–vis spectra of solutions were recorded on a Perkin-Elmer Lambda-750 using calibrated 0.2 cm Quartz-cell.

2.9. Elemental analysis

C, H, and N elemental analyses were carried out by BioCIS-UMR 8076 Service Chromato-Masse Microanalyse Faculté de Pharmacie Tour D5-5ème étage 5 avenue JB Clément 92290 CHÂTENAY-MALABRY. Na and V contents were determined by Inductively Coupled Plasma optical emission spectroscopy (ICP-AES) using an Agilent 720 Series with axially-viewed plasma and Na/V calibration curves.

3. Results and discussion

3.1. Synthesis

The hybrid hexavanadate $[V_6O_{13}\{(OCH_2)_3C–NH(BOC)\}_2]^{2-}$ was prepared in two steps (Figure 1). The first one consists in the preparation of the tert-butyl N-[1,3-dihydroxy-2-(hydroxymethyl)propan-2-yl]carbamate that can be easily prepared in very good yield (100%) from the reaction of tert-butyloxycarbonyl with di-tert-butyl dicarbonate in methanol [37]. The second synthetic step is inspired by the procedures allowing the formation of the various hybrid Lindqvist-type POV involving the reaction of the deca-vanadate (TBA)$_3$[H$_3$V$_{10}$O$_{28}$] with the desired Triol-ligands in hot N,N-dimethylacetamide.
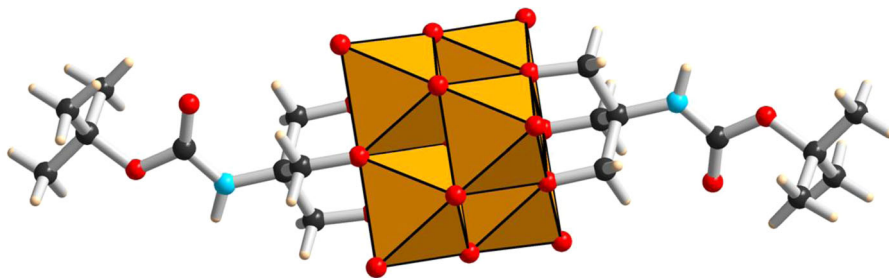
Figure 2. Structural view of $[V_6O_{13}\{(OCH_2)_3C-NH(BOC)\}_2]^{2-}$. Orange polyhedron: VO_6; red sphere: oxygen; black sphere: carbon; blue sphere: nitrogen; light pink sphere: hydrogen.

Adapting this synthetic route, we prepared in good yield (50%) the desired compound, as demonstrated by structural characterization, FT-IR spectroscopy, and multinuclear NMR in solution.

3.2. Crystal structure

$(TBA)_2[V_6O_{13}\{(OCH_2)_3C-NH(BOC)\}_2]\cdot 2DMA$, notated **V$_6$-Tris-BOC**, crystallizes in the centrosymmetric space group $P2_1/c$ and the asymmetric unit contains half of the hybrid hexavanadate $[V_6O_{13}\{(OCH_2)_3C-NH(BOC)\}_2]^{2-}$, one TBA^+ cation, and one dimethylacetamide molecule of crystallization. The structure of the $[V_6O_{13}\{(OCH_2)_3C-NH(BOC)\}_2]^{2-}$ anion, shown in Figure 2, corresponds to the archetypical Lindqvist-type polyanion in which the six vanadium centers form an octahedron and two trialkoxo ligands occupy the opposite faces of the octahedron in *trans*-mode. An inversion center is located at the central μ_6-oxygen atoms of the POV. Within the inorganic core $\{V_6O_{19}\}^{8-}$, each vanadium has a distorted octahedral geometry in which the shortest and longest V–O distances are observed with the terminal oxygen O^t (1.600(2)–1.606(2) Å) and the central μ_6-oxygen atom (2.2251(4)–2.2492(4) Å), respectively. The bond length between the vanadium ions and bridging μ_2-oxygen is 1.802(2)–1.854(2) Å, while the V–O distances observed with the alkoxy bridging μ_2-oxygen is slightly longer (2.000(2)–2.038(2) Å). The geometric parameters of the inorganic core in **V$_6$-Tris-BOC** are similar to those previously observed in equivalent Tris-derivative hexavanadate $[V_6O_{13}\{(OCH_2)_3CNH_2\}_2]^{2-}$ [33].

The three-dimensional cohesion is insured mainly by a network of short contacts and hydrogen bonds (Figure 3). The inorganic core of $[V_6O_{13}\{(OCH_2)_3C-NH(BOC)\}_2]^{2-}$ is surrounded by four tetrabutylammonium cations interacting through numerous short contacts ($d_{C-H\cdots O-V}$ = 2.38–2.80 Å) between the hydrogens of alkyl tails and the oxygens located at the surface of the $\{V_6O_{19}\}^{8-}$ motif (Figure 3(A)). Such an organization involves formation of a neutral chain $\{TBA_2[V_6O_{13}\{(OCH_2)_3C-NH(BOC)\}_2]\}$ along the *b* axis where the $\{V_6O_{19}\}^{8-}$ motifs are separated by a pair of TBA cations. Such chains are connected in the *ab* plane by intercalated solvent molecules (DMA) of crystallization (two DMA per POV unit). Each DMA molecule interacts with one POV by one hydrogen bond between the oxygen atom of the DMA and the N–H group of POV ($d_{N-H\cdots O-C}$ = 2.221(4) Å) and with another POV by short contact ($d_{C-H\cdots O-V}$ = 2.561(2) Å) (Figure 3(B)). From this organization, the formation of layers is stacked
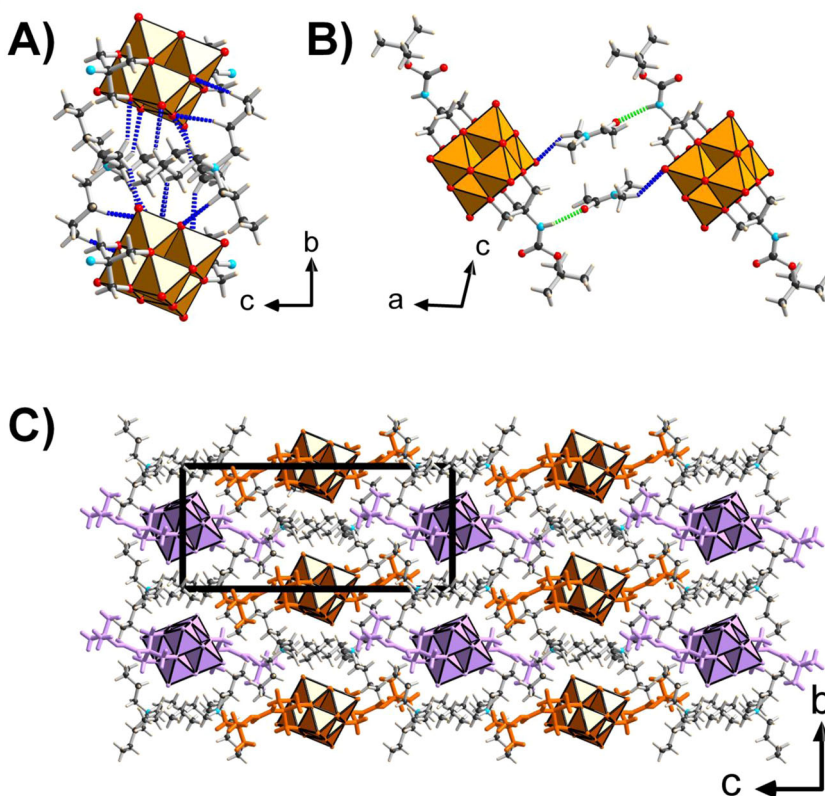
Figure 3. A) Illustration of the short contacts occurring between POVs and TBA$^+$ showing a pair of TBA$^+$ connecting two POVs along the b axis. Dotted blue lines: short contacts between the hydrogens of the alkyl chains of TBA$^+$ and the oxygens located at the surface of the POV. The BOC chain is omitted for clarity. B) Illustration of the supramolecular interaction between the POV and the DMA. Dotted green lines: hydrogen bonds between the NH groups of the POV-Tris and the oxygen atom of the DMA. Dotted blue lines: short contacts between hydrogens of DMA and terminal oxygens of the POV. C) Illustration of the packing along the a axis, showing the stacking of the layer along the c axis. To highlight the two different layers, two colors have been used for the POVs. DMA molecules have been omitted for clarity.

along the c axis, with 180° rotation and a shift of $b/2$ from one to the other. The organic tails of the $[V_6O_{13}\{(OCH_2)_3C-NH(BOC)\}_2]^{2-}$ anion point upward and downward to two adjacent layer planes, generating van der Waals interactions between the layers that ensure the 3D cohesion of the crystal structure (Figure 3(C)).

3.3. FT-IR spectroscopy

Figure S8 shows the FT-IR spectrum of $(TBA)_2[V_6O_{13}\{(OCH_2)_3C-NH(BOC)\}_2]\cdot2DMA$. The three characteristic features of the inorganic core $\{V_6O_{19}\}^{8-}$ are located at 949, 805, and 720 cm^{-1}. The strong peak at 949 cm^{-1} corresponds to the $V=O^t$ (terminal oxygen atoms) vibration. The two other peaks are attributed to vibrations of $V-O^b-V$ that involves bridging oxygens of the metal-oxo framework. Numerous strong IR absorptions of the organic part of the hybrid hexavanadate, the DMA and the TBA cations
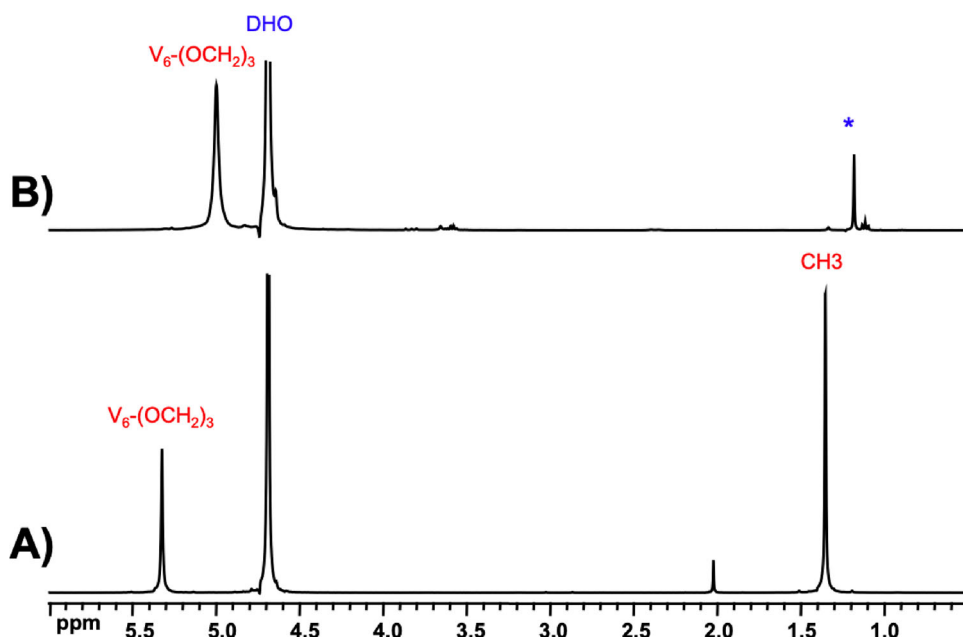
Figure 4. ^{1}H NMR spectra of A) Na$_2$[V$_6$O$_{13}${(OCH$_2$)$_3$C–NH(BOC)}$_2$] in D$_2$O and B) [V$_6$O$_{13}${(OCH$_2$)$_3$C–NH$_3$}$_2$] in D$_2$O/NaOD. (*) denotes residual BOC (7%).

are observed at 1000–1650 cm^{-1}, however, the identification of all peaks is challenging. The broad C=O stretching peaks at 1706 and 1642 cm^{-1} can be attributed to the amide groups of the ligand {(OCH$_2$)$_3$C–NH(BOC)} and the DMA, respectively. The peaks at 1472, 1400, and 1370 cm^{-1} are assigned to asymmetric and symmetric deformations of the C–H of the methyl and methylene groups of the TBA cation, the ligand, and the DMA. Asymmetric and symmetric vibrations of C–H are observed at 2873 and 2964 cm^{-1}.

3.4. NMR spectroscopy

(TBA)$_2$[V$_6$O$_{13}${(OCH$_2$)$_3$C–NH(BOC)}$_2$]·2DMA has been characterized by ^{1}H, ^{13}C{^{1}H}, and ^{51}V NMR in acetonitrile (ACN). The ^{51}V NMR spectrum (Supporting Information, Figure S1) exhibits a single resonance at −497 ppm (half-height line width δ $\nu_{1/2}$ *ca.* 400 Hz) indicating a highly symmetric POV, consistent with a *trans*-coordination mode. Similar result was observed with [V$_6$O$_{13}${(OCH$_2$)$_3$C–N(4-CONHC$_5$H$_4$N)}$_2$]$^{2-}$ (−495 ppm/DMSO-d$_6$) [20]. The ^{1}H NMR spectrum (Supporting Information, Figure S1) confirms the grafting of organic moieties on the surface of the POV showing the signals of methylenic protons V$_6$-(OCH$_2$)$_3$ and methyl groups of Tris-BOC at 5.16 and 1.38 ppm, respectively. Signals of TBA cations at 0.99, 1.45, 1.60, and 3.16 ppm, and of DMA crystallization solvent at 1.98, 2.84, and 2.97 ppm are also identified. Integration of these signals reveals molar ratios Tris-BOC/TBA/DMA = 1/1/1, consistent with a global POV charge of 2- and co-crystallization of 2 DMAC molecules with one POV unit as determined by XRD analysis. ^{13}C NMR spectrum (Supporting Information, Figure S2) shows the
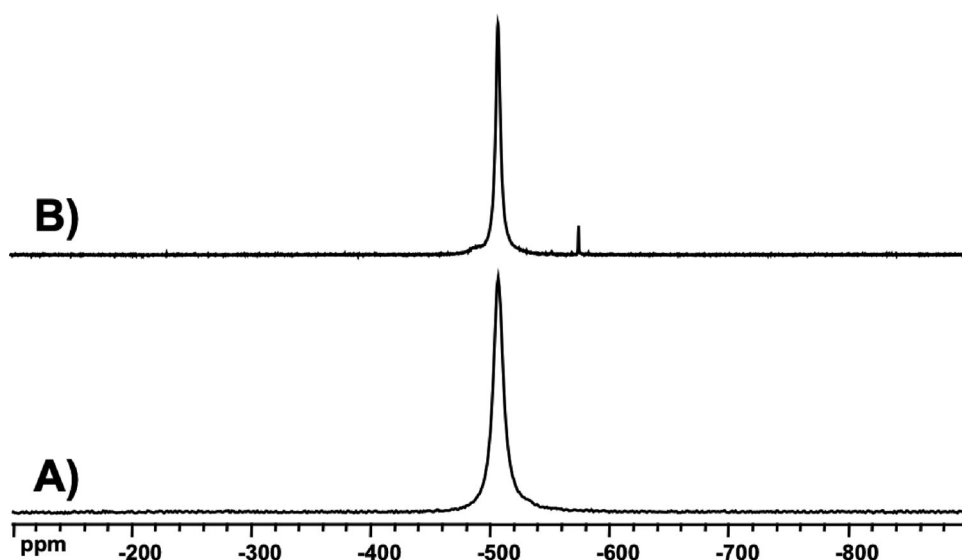
Figure 5. ^{51}V NMR spectra of A) $Na_2[V_6O_{13}\{(OCH_2)_3C–NH(BOC)\}_2]$ in D_2O and B) $[V_6O_{13}\{(OCH_2)_3C–NH_3\}_2]$ in $D_2O/NaOD$.

resonances of Tris-BOC moieties at 28.3, 52.1, 83.7, 87.2, and 155.5 ppm. The overall NMR data are in agreement with pure and stable compound in acetonitrile.

$(TBA)_2[V_6O_{13}\{(OCH_2)_3C–NH(BOC)\}_2]·2DMA$ is not soluble in aqueous solution. However, the exchange of counter cations TBA^+ by sodium allows solubilizing the hybrid POV $Na_2[V_6O_{13}\{(OCH_2)_3C–NH(BOC)\}_2]·6H_2O$ in water. Hydrolysis of the peptidic function is therefore achieved in acidic medium using HCl, which provokes an immediate precipitation. The resulting solid consists of the neutral protonated form, $[V_6O_{13}\{(OCH_2)_3C–NH_3\}_2]$. Figure 4(A) shows the ^1H NMR spectra of $Na_2[V_6O_{13}\{(OCH_2)_3C–NH(BOC)\}_2]$ and $[V_6O_{13}\{(OCH_2)_3C–NH_3\}_2]$ in D_2O. The spectrum of $Na_2[V_6O_{13}\{(OCH_2)_3 C–NH(BOC)\}_2]$ exhibits the signals of CH_2 of Tris moieties at 5.32 ppm and of the methyl groups of the BOC at 1.32 ppm. To verify that the BOC is still attached to the POV upon its dissolution in aqueous solution, DOSY NMR is carried out. The spectrum shown in Supporting Information (Figure S3) reveals that the two organic parts (Tris and BOC) diffuse with the same rate at 295 μm²/s. This proves that the Tris–BOC is robust and remains intact in aqueous solution, and then acidic protons are needed to hydrolyze the amide function. The neutral solid product $[V_6O_{13}\{(OCH_2)_3C–NH_3\}_2]$ is insoluble in water and deprotonation of ammonium groups is needed to solubilize it. Therefore, NMR measurements were conducted in basic medium (NaOD/D_2O). The ^1H NMR spectrum (Figure 4(B)) shows the signal of CH_2 of the Tris at 5.00 ppm and a small signal at *ca.* 1.2 ppm accounting for residual BOC. DOSY NMR (Supporting Information, Figure S4) confirms the assignments where two distinct diffusion rates are measured at 422 and 758 μm²/s for the POV–Tris and BOC, respectively. ^{13}C NMR (Supporting Information, Figures S5 and S6) provides further support of ^1H assignments of $Na_2[V_6O_{13}\{(OCH_2)_3C–NH(BOC)\}_2]$ and $[V_6O_{13}\{(OCH_2)_3C–NH_3\}_2]$. To provide definitive proof of hydrolysis of the amide function, ^{15}N NMR has been carried out. The $^{15}N\{^1H\}$ HMBC (Supporting Information,
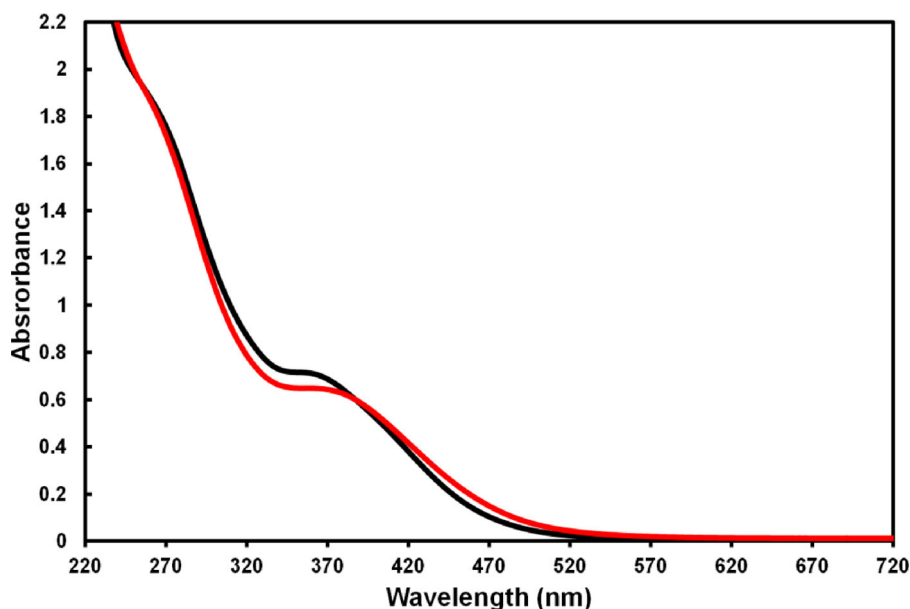
Figure 6. UV–vis spectra of $TBA_2[V_6O_{13}\{(OCH_2)_3C–NH(BOC)\}_2]\cdot 2DMA$ in MeCN (black line) and $Na_2[V_6O_{13}\{(OCH_2)_3C–NH(BOC)\}_2]\cdot 6H_2O$ in water (red line).

Figure S7) reveals that the initial signal of the amide function in $[V_6O_{13}\{(OCH_2)_3C–NH(BOC)\}_2]^{2-}$ at −290.7 ppm shifts to −352.8 ppm, corresponding to typical chemical shift ranges for amines. Finally, the ^{51}V NMR spectra (Figure 5) of $Na_2[V_6O_{13}\{(OCH_2)_3C–NH(BOC)\}_2]$ and $[V_6O_{13}\{(OCH_2)_3C–NH_3\}_2]$ are comparable, exhibiting a broad resonance at *ca.* −507 ppm (half-height line widths $\delta\ \nu_{1/2} \sim$ 500–1000 Hz). This signature is typical of Lindqvist-type structure.

3.5. UV–vis spectroscopy

The UV–vis spectrum of $[V_6O_{13}\{(OCH_2)_3C–NH(BOC)\}_2]^{2-}$ has been measured in acetonitrile using the TBA^+ salt. This spectrum exhibits two strong absorption bands at 262 and 365 nm (Figure 6), and the corresponding molar extinction coefficients are 20,300 and 8465 $M^{-1} cm^{-1}$, respectively. These values are in the same range as those observed by Zubieta on various hexavanadates [19]. These absorption bands are attributed to the oxygen to metal charge transfer transition. The UV–vis spectrum of $[V_6O_{13}\{(OCH_2)_3C–NH(BOC)\}_2]^{2-}$ has also been measured in aqueous media using the sodium salt. The spectrum exhibits similar features even if a slight red-shift (+10 nm) is observed, indicating a solvent dependence of the absorptions position.

4. Conclusion

We have synthesized a new tris(hydroxymethyl)aminomethane (Tris) based functionalized Lindqvist-type hexavanadate, $TBA_2[V_6O_{13}\{(OCH_2)_3C–NH(BOC)\}_2]$, using N-tert-butoxycarbonyl (BOC) as protecting group of the Tris amine function. The compound has been characterized by single-crystal XRD and FT-IR spectroscopy in the solid state

as well as UV–vis and multinuclear NMR spectroscopies in solution. The sodium salt obtained by cationic exchange is found highly soluble and stable in aqueous solution, which allows deprotection of the amine group to obtain the dianion $[V_6O_{13}\{(OCH_2)_3C-NH_2\}_2]^{2-}$. This new synthetic method offers a simplified procedure for obtaining Tris-Lindqvist vanadate anion with good yield.

Disclosure statement

No potential conflict of interest was reported by the authors.

Funding

References

[1]   J. Livage. *Coord. Chem. Rev.*, **178–180**, 999 (1998).

[2]   K.Y. Monakhov, W. Bensch, P. Kogerler. *Chem. Soc. Rev.*, **44**, 8443 (2015).

[3]   L.E. VanGelder, T.R. Cook, E.M. Matson. *Comments Inorg. Chem.*, **39**, 51 (2019).

[4]   L.E. VanGelder, A.M. Kosswattaarachchi, P.L. Forrestel, T.R. Cook, E.M. Matson. *Chem. Sci.*, **9**, 1692 (2018).

[5]   L.E. VanGelder, B.E. Petel, O. Nachtigall, G. Martinez, W.W. Brennessel, E.M. Matson. *ChemSusChem*, **11**, 4139 (2018).

[6]   L.E. VanGelder, E. Schreiber, E.M. Matson. *J. Mater. Chem. A*, **7**, 4893 (2019).

[7]   J.J. Chen, M.D. Symes, S.C. Fan, M.S. Zheng, H.N. Miras, Q.F. Dong, L. Cronin. *Adv. Mater. Weinheim*, **27**, 4649 (2015).

[8]   J.J. Chen, J.C. Ye, X.G. Zhang, M.D. Symes, S.C. Fan, D.L. Long, M.S. Zheng, D.Y. Wu, L. Cronin, Q.F. Dong. *Adv. Energy Mater.*, **8**, 1701021 (2018).

[9]   S. Greiner, M.H. Anjass, M. Fichtner, C. Streb. *Inorg. Chem. Front.*, **7**, 134 (2020).

[10]   S.S. Lu, Y. Lv, W.Q. Ma, X.F. Lei, R.E. Zhang, H. Liu, X.Z. Liu. *Inorg. Chem. Front.*, **4**, 2012 (2017).

[11]   B. Schwarz, J. Forster, M.H. Anjass, S. Daboss, C. Kranz, C. Streb. *Chem. Commun. (Camb.)*, **53**, 11576 (2017).

[12]   B. Schwarz, J. Forster, M.K. Goetz, D. Yucel, C. Berger, T. Jacob, C. Streb. *Angew. Chem. Int. Ed. Engl.*, **55**, 6329 (2016).

[13]   C. Li, N. Mizuno, K. Murata, K. Ishii, T. Suenobu, K. Yamaguchi, K. Suzuki. *Green Chem.*, 3896 (2020).

[14]   B.E. Petel, W.W. Brennessel, E.M. Matson. *J. Am. Chem. Soc.*, **140**, 8424 (2018).

[15]   B.E. Petel, A.A. Fertig, M.L. Maiola, W.W. Brennessel, E.M. Matson. *Inorg. Chem.*, **58**, 10462 (2019).

[16]   B.E. Petel, R.L. Meyer, M.L. Maiola, W.W. Brennessel, A.M. Muller, E.M. Matson. *J. Am. Chem. Soc.*, **142**, 1049 (2020).

[17]   A.V. Anyushin, A. Kondinski, T.N. Parac-Vogt. *Chem. Soc. Rev.*, **49**, 382 (2020).

[18]   J.W. Zhang, Y.C. Huang, G. Li, Y.G. Wei. *Coord. Chem. Rev.*, **378**, 395 (2019).

[19]   Q. Chen, D.P. Goshorn, C.P. Scholes, X.L. Tan, J. Zubieta. *J. Am. Chem. Soc.*, **114**, 4667 (1992).

[20]   J.W. Han, K.I. Hardcastle, C.L. Hill. *Eur. J. Inorg. Chem.*, **2006**, 2598 (2006).

[21] D. Li, J. Song, P.C. Yin, S. Simotwo, A.J. Bassler, Y.Y. Aung, J.E. Roberts, K.I. Hardcastle, C.L. Hill, T.B. Liu. *J. Am. Chem. Soc.*, **133**, 14010 (2011).
[22] P.C. Yin, A. Bayaguud, P. Cheng, F. Haso, L. Hu, J. Wang, D. Vezenov, R.E. Winans, J. Hao, T. Li, Y.G. Wei, T.B. Liu. *Chemistry*, **20**, 9589 (2014).
[23] P.C. Yin, J. Wang, Z.C. Xiao, P.F. Wu, Y.G. Wei, T.B. Liu. *Chemistry*, **18**, 9174 (2012).
[24] P.C. Yin, P.F. Wu, Z.C. Xiao, D. Li, E. Bitterlich, J. Zhang, P. Cheng, D.V. Vezenov, T.B. Liu, Y.G. Wei. *Angew. Chem. Int. Ed. Engl.*, **50**, 2521 (2011).
[25] Y.T. Zhu, Y.C. Huang, Q. Li, D.J. Zang, J. Gu, Y.J. Tang, Y.G. Wei. *Inorg. Chem.*, **59**, 2575 (2020).
[26] Q. Chen, J. Zubieta. *Inorg. Chim. Acta*, **198**, 95 (1992).
[27] Q. Chen, J. Zubieta. *Inorg. Chem.*, **29**, 1456 (1990).
[28] A. Müller, J. Meyer, H. Bögge, A. Stammler, A. Botar. *Z Anorg. Allg. Chem.*, **621**, 1818 (1995).
[29] A. Bayaguud, K. Chen, Y.G. Wei. *Nano Res.*, **9**, 3858 (2016).
[30] Z.C. Xiao, K. Chen, B.L. Wu, W.J. Li, P.F. Wu, Y.G. Wei. *Eur. J. Inorg. Chem.*, **2016**, 808 (2016).
[31] A. Bayaguud, J. Zhang, R.N.N. Khan, J. Hao, Y.G. Wei. *Chem. Commun. (Camb.)*, **50**, 13150 (2014).
[32] B.F. Zhang, J. Song, D. Li, L. Hu, C.L. Hill, T.B. Liu. *Langmuir*, **32**, 12856 (2016).
[33] A. Bayaguud, K. Chen, Y.G. Wei. *Cryst. Eng. Comm.*, **18**, 4042 (2016).
[34] U. Ragnarsson, L. Grehn. *RSC Adv.*, **3**, 18691 (2013).
[35] J. Selambarom, S. Monge, F. Carre, J.P. Roque, A.A. Pavia. *Tetrahedron*, **58**, 9559 (2002).
[36] V.W. Day, W.G. Klemperer, D.J. Maltbie. *J. Am. Chem. Soc.*, **109**, 2991 (1987).
[37] R. Kaplanek, T. Briza, M. Havlik, P. Martasek, V. Kral. *J. Fluor. Chem.*, **128**, 179 (2007).
[38] O.V. Dolomanov, L.J. Bourhis, R.J. Gildea, J.A.K. Howard, H. Puschmann. *J. Appl. Crystallogr.*, **42**, 339 (2009).
[39] G.M. Sheldrick. *Acta Crystallogr. C Struct. Chem.*, **71**, 3 (2015).
[40] G.M. Sheldrick. *Acta Crystallogr. A Found Adv.*, **71**, 3 (2015).
[41] M.A. Delsuc, T.E. Malliavin. *Anal. Chem.*, **70**, 2146 (1998).